Enforcing the Discrete Maximum Principle for Linear Finite Element Solutions of Second-Order Elliptic Problems

Richard Liska[1,*] and Mikhail Shashkov[2]

[1] *Czech Technical University in Prague, Faculty of Nuclear Sciences and Physical Engineering, Břehová 7, 115 19 Prague 1, Czech Republic.*
[2] *Theoretical Division, Group T-7, MS-B284, Los Alamos National Laboratory, Los Alamos, NM 87545, USA.*

Abstract. The maximum principle is a basic qualitative property of the solution of second-order elliptic boundary value problems. The preservation of the qualitative characteristics, such as the maximum principle, in discrete model is one of the key requirements. It is well known that standard linear finite element solution does not satisfy maximum principle on general triangular meshes in 2D. In this paper we consider how to enforce discrete maximum principle for linear finite element solutions for the linear second-order self-adjoint elliptic equation. First approach is based on repair technique, which is a posteriori correction of the discrete solution. Second method is based on constrained optimization. Numerical tests that include anisotropic cases demonstrate how our method works for problems for which the standard finite element methods produce numerical solutions that violate the discrete maximum principle.

AMS subject classifications: 35J25, 65N99

Key words: Second-order elliptic problems, linear finite element solutions, discrete maximum principle, constrained optimization.

1 Introduction

In this paper we consider two approaches to enforce discrete maximum principle for linear finite element solution of the linear second-order self-adjoint elliptic equation without lower-order terms.

---

*Corresponding author. *Email addresses:* `liska@siduri.fjfi.cvut.cz` (R. Liska), `shashkov@lanl.gov` (M. Shashkov)

It is well known that standard finite element methods can for some problems produce numerical solutions violating a discrete maximum principle (DMP) which is the discrete analog of the maximum principle, see, e.g., [1–7]. In the classical paper [8] Ciarlet and Raviart show that for the case of scalar isotropic diffusion coefficient the standard linear finite element method applied to Poisson equation satisfies the DMP on weakly acute triangular meshes. The weakly acute geometric condition is a typical condition under which some numerical methods produce solutions satisfying the DMP. The uniform constant anisotropic diffusion tensor can be transformed to the isotropic tensor (or the scalar diffusion coefficient) by rotating and scaling the coordinate system, so that one can use the acute conditions in the transformed coordinates. However, often one cannot choose the computational mesh or the anisotropy ratio is too big to provide a practical computational acute mesh in the transformed coordinates.

The issues related to the DMP have been studied by many researches. Here we try to review the recent contributions in the issues. The DMP for stationary heat conduction in nonlinear, inhomogeneous, and anisotropic media is analyzed by Krizek and Liu in [9, 10]. The dependence of DMP on mesh properties for finite element solutions of elliptic problems with mixed boundary conditions is considered by Karatson and Korotov in [11, 12]. Burman and Ern [13] have developed a nonlinear stabilized Galerkin approximation of the Laplace operator whose solutions satisfy the DMP without the need to satisfy the acute condition. However, this requires solving a nonlinear system of equations instead of a standard linear one. Le Potier has proposed a finite volume scheme for highly anisotropic diffusion problems on unstructured meshes [2] and improved it to the nonlinear version [3] which is monotone for a parabolic problem with sufficiently small time step. It has been further improved by Lipnikov et al. in [6], resulting in a nonlinear monotone finite volume scheme for elliptic problems which keeps positivity of the solution, however, can still violate the DMP. Mlacnik and Durlofsky [5] perform mesh optimization to improve the monotonicity of the numerical solution for highly anisotropic problems. A new mixed finite volume scheme for anisotropic diffusion problems has been developed by Droniou and Eymard in [4], however, it does not satisfy the DMP for highly anisotropic problems. The DMP has been investigated by means of discrete Green's function positivity by Draganescu et al. in [1]. The DMP for 1D problems with discontinuous coefficients is studied by Vejchodsky and Solin in [14]. The criteria for the monotonicity of control volume methods on quadrilateral meshes are derived by Nordbotten et al. in [7]. The elliptic solver on Cartesian grids for interface problems by Deng et al. [15] uses the standard scheme away from the interface, and a positive scheme at the interface is derived by using constrained optimization techniques. Hoteit et al. [16] study how to avoid violation of the DMP by the mixed-hybrid finite-element method (MHFEM) applied to a parabolic diffusion problem and propose two techniques reducing the MHFEM to finite difference methods obeying the DMP.

Our first approach to enforce discrete maximum principle is based on repair technique, [20–22], which is a posteriori correction of the discrete solution. Second method is based on constrained optimization. The quadratic optimization problem is related to

variational formulation of elliptic boundary value problem and linear constraints are explicitly introduced to satisfy discrete maximum principle.

In Section 2, we introduce the discrete maximum principle for the second-order elliptic equation with Dirichlet boundary conditions. In Section 3 we describe two new methods for enforcing discrete maximum principle. We start with addressing an issue of keeping the solution conservative in Section 3.1. The we describe a repair technique in Section 3.2. Method based on constrained optimization is described in Section 3.3. Several problems (most with strong anisotropy), for which the standard linear finite element method violates the DMP while our approach gives numerical solution satisfying the DMP, are presented in Section 4 for homogeneous elliptic equations and in Section 5 for non-homogeneous equations. Some future plans are described in Section 6.

2 Linear self-adjoint second-order elliptic boundary value problem: Maximum principle and discrete maximum principle

We will consider linear self-adjoint second-order elliptic boundary value problem without low order terms:

$$
\begin{aligned}
-Lu &= -\mathrm{div}\left(\mathbf{A}\cdot\mathbf{grad}\,u(\mathbf{x})\right) = f(\mathbf{x}), \quad \mathbf{x}\in\Omega, \\
u(\mathbf{b}) &= \psi(\mathbf{b}), \quad \mathbf{b}\in\partial\Omega,
\end{aligned}
\tag{2.1}
$$

where the matrix $\mathbf{A}(\mathbf{x})$

$$
\mathbf{A} = \begin{pmatrix} a_{11} & a_{12} \\ a_{12} & a_{22} \end{pmatrix}
\tag{2.2}
$$

is a symmetric positive definite diffusion matrix:

$$
\sum_{\alpha,\beta=1,2} a_{\alpha,\beta}(x,y)\xi_\alpha\xi_\beta > 0, \quad \forall\,\boldsymbol{\xi} = (\xi_1,\xi_2)\ \text{with}\ |\boldsymbol{\xi}|\neq 0,\ \text{and}\ \forall\,(x,y)\in\overline{\Omega},
\tag{2.3}
$$

and $f(\mathbf{x})$ is given function. We will assume that a_{11},a_{12},a_{22},f are bounded functions from $L^2(\Omega), \psi\in C(\partial\Omega)$, and $\Omega\subset R^2$ is bounded domain with Lipschitz-continuous polygonal boundary $\partial\Omega$.

The maximum principle for an elliptic differential operator L is an important notion for elliptic problems. It states, see, e.g. [17], that if a function $u(\mathbf{x})$ satisfies $Lu(\mathbf{x})\geq 0$ for $\mathbf{x}$ in a bounded domain Ω then $u(\mathbf{x})$ has the maximum value on the boundary $\partial\Omega$ of Ω and vise versa. If $f(\mathbf{x})\leq 0$ for all $\mathbf{x}\in\Omega$, then the maximum principle states that $u(\mathbf{x})$ has the maximum on the boundary, so that

$$
\forall\mathbf{x}\in\Omega, \quad u(\mathbf{x})\leq \max_{\mathbf{b}\in\partial\Omega}\psi(\mathbf{b}).
\tag{2.4}
$$

If $f(\mathbf{x}) \geq 0$ for all $\mathbf{x} \in \Omega$, then the maximum principle states that $u(\mathbf{x})$ has the minimum on the boundary, so that

$$\forall \mathbf{x} \in \Omega, \quad u(\mathbf{x}) \geq \min_{\mathbf{b} \in \partial \Omega} \psi(\mathbf{b}). \tag{2.5}$$

For the homogeneous equation, i.e., zero source $f(\mathbf{x}) = 0$, the maximum principle implies that the value of the solution of problem (2.1) $u(\mathbf{x})$ at any internal point $\mathbf{x}$ of Ω is bounded by extremal boundary values ψ, so that

$$\forall \mathbf{x} \in \Omega, \quad \min_{\mathbf{b} \in \partial \Omega} \psi(\mathbf{b}) \leq u(\mathbf{x}) \leq \max_{\mathbf{b} \in \partial \Omega} \psi(\mathbf{b}). \tag{2.6}$$

When the source f changes the sign inside the domain Ω then the solution of the elliptic equation (2.1) might have local extrema inside the domain Ω.

We will consider discretization of (2.1) on triangular mesh in 2D domain Ω, where the functions $u(\mathbf{x}), f(\mathbf{x})$ have discrete values U_n, F_n at the mesh nodes n, and coefficients of the matrix A are defined at triangles, for example, $a_{11,T}$. We will use standard linear finite element method (FEM). It is well known that under some assumptions about mesh regularity the solution of the standard linear FEM converges to the solution of the Dirichlet problem (2.1) with mesh refinement [19].

The discrete version of the maximum principle (2.4) for non-positive sources ($\forall n, F_n \leq 0$) states that for all nodes n

$$\forall n, \ U_n \leq \max_{\mathbf{x}_j \in \partial \Omega} \Psi_j, \tag{2.7}$$

where for the boundary nodes $\mathbf{b}_j \in \partial \Omega$ the discrete Dirichlet boundary conditions are given by $\Psi_j = \psi(\mathbf{b}_j)$. The discrete version of the maximum principle (2.5) for non-negative sources ($\forall n, F_n \geq 0$) states that for all nodes n

$$\forall n, \ U_n \geq \min_{\mathbf{x}_j \in \partial \Omega} \Psi_j. \tag{2.8}$$

Finally, the discrete version of the maximum principle (2.6) for the homogeneous case states that for all nodes n

$$\forall n, \ \min_{\mathbf{x}_j \in \partial \Omega} \Psi_j \leq U_n \leq \max_{\mathbf{x}_j \in \partial \Omega} \Psi_j. \tag{2.9}$$

As will be seen below, in the numerical tests there exist problems for which the unbounded solution U^u does not satisfy one of the discrete maximum principles.

3 Enforcing the discrete maximum principle

In this section we describe two methods to enforce discrete maximum principle. First approach is based on repair technique, [20–22], which is a posteriori correction of the discrete solution. The repair procedure allows to correct discrete solution in such a way that discrete energy of the solution is preserved. Second method is based on constrained optimization. The quadratic optimization problem is related to the variational formulation of the elliptic boundary value problem and appropriate linear constraints (2.7), (2.8), or (2.9) are explicitly introduced to satisfy discrete maximum principle.

3.1 Notion of the conservation

Elliptic equation can be interpreted as a stationary heat equation with u being temperature. In this case, the total heat energy $\int_\Omega u\,dV$ is in the discrete case approximated by

$$E[U] = \sum_n U_n V_n, \tag{3.1}$$

where the summation goes over all nodes of the computational mesh, and V_n is the volume associated with the node n defined as one third of the sum of areas of all triangles which have node n as one of their vertices (this definition is the same as if we add from each triangle the area of quadrilateral created by the node, triangle center, and centers of two corresponding edges). In some application it maybe important to have some notion of preservation of total energy when modifying discrete solution to satisfy maximum principle. In this paper, we define the total energy which we want to preserve using linear finite element solution. It is denoted by U^u, where the superscript stands for *unbounded*, because it can violate bounds defined by the discrete maximum principle. One can choose also another sample solution obtained, e.g., by some other higher order numerical method. The total energy is $E[U^u]$, and we require that the modified solution $\tilde U$ has the same total energy, i.e.,

$$E[\tilde U] = E[U^u] = \sum_n U_n^u V_n, \tag{3.2}$$

where U_n^u is the value of the unbounded solution at the node n.

3.2 Repair

We repair the nodal values of U^u violating the given discrete maximum principle by redistributing the heat energy to or from their neighbors so that (3.2) remains valid.

Let us assume that the unbounded solution at node n violates the minimum constraint (2.8), so that

$$U_n < U^{min} = \min_{\mathbf{x}_m \in \partial\Omega} \Psi_m$$

(in the description of the repair we drop the superscript u denoting the unbounded solution). To correct this violation of lower bound, we need to add the needed energy

$$\Delta E = (U^{min} - U_n) V_n$$

to the node n. We denote by $N(n)$ the set of nodes neighboring the node n (each neighboring node defines one edge connecting this node with the node n). For all neighboring nodes $m \in N(n)$, the available energy E_m^a at node m which can be taken out of this node and given to the node n (without violating the minimum constraint (2.8) at node m) is

$$E_m^a = \max(0, (U_m - U^{min}) V_m)$$

and it is positive if $U_m > U^{min}$. The total available energy in all the neighboring nodes is

$$E^a = \sum_{m \in N(n)} E^a_m.$$

Now, if the total available energy is greater than the needed energy, i.e., $E^a \geq \Delta E$, we have enough available energy to correct the temperature in the node n to its minimal value U^{min}. We set $U^r_n = U^{min}$ (superscript r refers to "repaired" value of the temperature) and take out the needed energy ΔE from neighbors in proportion to what they can give, which leads to the following formula

$$U^r_m := \frac{U_m V_m - E^a_m (\Delta E / E^a)}{V_m}, \quad \forall m \in N(n),$$

so that the total energy (3.2) remains constant (see [20] for detail).

On the other hand if the total available energy is less than the needed energy, we extend the neighborhood $N(n)$ by the neighbors of all nodes from $N(n)$ and repeat the outlined procedure. The repair procedure is applied to all nodes violating the lower bound (2.8).

When the upper bound on the solution (2.7) is not valid, the repair of temperature at nodes violating the upper bound proceeds in a similar way as the repair of temperature at nodes violating the lower bound (2.8) described above. The solution obtained by repair is called *repaired* solution and is denoted by U^r.

3.3 Constrained optimization

Under some assumptions about smoothness of the coefficients and right-hand side function, problem (2.1) is equivalent to minimization of the energy functional

$$\begin{aligned}
\mathcal{F}[u] &= \int_\Omega (\mathbf{grad}\, u \cdot (\mathbf{A} \cdot \mathbf{grad}\, u) - 2f(\mathbf{x})u(\mathbf{x})) \, dV, \\
u(\mathbf{b}) &= \psi(\mathbf{b}), \quad \mathbf{b} \in \partial\Omega.
\end{aligned} \tag{3.3}$$

Standard linear finite element solution can be obtained by minimizing discrete analog of optimization problem (3.3). For discrete approximation of the gradient $\mathbf{grad}\, u$ in the triangle T defined by three counter-clockwise numbered nodes $(x^T_1, y^T_1), (x^T_2, y^T_2), (x^T_3, y^T_3)$ we use, see [18],

$$GRAD^x_T(U) = \frac{1}{2V_T} \Big((U^T_1 + U^T_2)(y^T_2 - y^T_1) + (U^T_2 + U^T_3)(y^T_3 - y^T_2) + (U^T_3 + U^T_1)(y^T_1 - y^T_3) \Big),$$

$$GRAD^y_T(U) = -\frac{1}{2V_T} \Big((U^T_1 + U^T_2)(x^T_2 - x^T_1) + (U^T_2 + U^T_3)(x^T_3 - x^T_2) + (U^T_3 + U^T_1)(x^T_1 - x^T_3) \Big),$$

where V_T is the area of the triangle T and U_1^T, U_2^T, U_3^T are discrete values of $u(\mathbf{x})$ at corresponding nodes of the triangle T. The discrete energy functional is now given by

$$\mathcal{F}_h[U] = \sum_T \Big[\big(a_{11,T} GRAD_T^x(U) + a_{12,T} GRAD_T^y(U) \big) GRAD_T^x(U) + \big(a_{12,T} GRAD_T^x(U)$$

$$+ a_{22,T} GRAD_T^y(U) \big) GRAD_T^y(U) - \frac{2}{3} F^T \sum_{j=1}^3 U_j^T \Big] V_T, \tag{3.4}$$

where the summation is over all mesh triangles covering the computational region Ω and $F^T = f(x^T, y^T)$ is the value of the source f at the center

$$(x^T, y^T) = \frac{1}{3} \sum_{j=1}^3 (x_j^T, y_j^T)$$

of the triangle T.

It is well known that the discrete function which delivers minimum to the functional (3.4) coincides with linear finite element solution of Eq. (2.1). We call this solution *unbounded*, since it is computed without imposing bounds on U_n, and denote it by U^u.

To enforce discrete maximum principle and to conserve the energy we suggest to minimize the discrete energy functional (3.4) under constraints corresponding to appropriate bounds (2.7) or (2.8) or (2.9) and the total energy constraint (3.2). This solution is called *constrained-bounded* solution and denoted by U^{cb}.

The discrete energy functional (3.4) is quadratic functional (with respect to $\{U_n\}$) with positive definite Hessian matrix, the maximum principle constraints (2.7) or (2.8) or (2.9) are just the interval for all discrete values U_n, and the total energy constraint (3.2) is linear in U_n, so we need to solve a convex quadratic programming problem. In our numerical experiments we are using Schittkowski convex quadratic programming package QL [23–25].

4   Numerical experiments for Laplace equation

In this section we present several numerical tests for the Laplace equation, i.e., for the Dirichlet problem for the Poisson equation (2.1) with zero source $f(\mathbf{x}) = 0$. The maximum principle for the Laplace equation is (2.6) and its discrete analogue is (2.9).

4.1   Two very simple problems

Here we present two very simple problems for Laplace equation with only two internal nodes, so the problems have only two unknowns U_1 and U_2 and their solutions can be illustrated in 2D $U_1 \times U_2$ space, so that one can easily see the features of different solutions. The first example produces the unbounded solution which violates the maximum principle (2.9), nevertheless, the constrained-bounded and repaired solutions do exist. The

second example also produces unbounded solution violating the maximum principle, however, this unbounded solution cannot be repaired. The repaired and constrained-bounded solutions (both conserving energy) do not exist.

The mesh for the first problem is presented in Fig. 1(a). The computational domain is the unit square $\Omega = [0,1] \times [0,1]$. The boundary conditions are specified as follows: $\psi = 0$ everywhere except $\psi = 4$ for $y = 0 \wedge x \in (0.1, 0.9)$ (so that the value $\psi = 4$ is set only for two central nodes on the lower edge). Different solutions of the first problem are plotted in Fig. 1(b) and the zoomed region of interest in Fig. 1(c). The solid line shows the box for U_1, U_2 unknowns given by the discrete maximum principle (2.9); the dashed line shows the total energy constraint (3.2). The unbounded solution

$$U^u = (U_1^u, U_2^u) \doteq (1.35, -0.11)$$

violates the minimum constraint $U_2 \geq 0$ for the unknown U_2, and as the unbounded solution defines the total energy, the unbounded solution U^u lies on the total energy constraint. The bounded solution $U^b \doteq (1.38, 0)$ lies on the boundary $U_2 = 0$ of U_2 lower constraint $U_2 \geq 0$. The constrained-bounded solution $U^{cb} \doteq (1.23, 0)$ which coincides with the repaired solution $U^r = U^{cb}$ is at the intersection of the total energy constraint with the boundary $U_2 = 0$ of U_2 lower constraint $U_2 \geq 0$. The discrete Dirichlet functional (3.4) values of the unbounded, bounded, repaired and constrained-bounded solutions are

$$\mathcal{F}_h[U^u] \doteq 44.41, \mathcal{F}_h[U^b] \doteq 44.51, \quad \mathcal{F}_h[U^r] = \mathcal{F}_h[U^{cb}] \doteq 44.62.$$

The total energy (3.1) of the unbounded, repaired, constrained-bounded and bounded solutions are

$$E[U^u] = E[U^r] = E[U^{cb}] \doteq 1.15, \quad E[U^b] \doteq 1.18.$$

The mesh for the second problem is presented in Fig. 2(a). The computational domain again is unit square $\Omega = [0,1] \times [0,1]$, and the boundary conditions are specified as follows: $\psi = 0$ everywhere except $\psi = 40$ for $y = 0 \wedge x \in (0.1, 0.9)$ (so that the value $\psi = 40$ is set only for two central nodes on the lower edge). Different solutions of the second problem are plotted in Fig. 2(b) and the zoomed region of interest in Fig. 2(c). The solid line shows the box for U_1, U_2 unknowns given by the discrete maximum principle (2.9), and the dashed line shows the total energy constraint (3.2). The total energy constraint does not intersect the maximum principle bounding box, which implies that the repaired and constrained-bounded solutions do not exist; so for this problem we have only the unbounded and bounded solutions. The unbounded solution

$$U^u = (U_1^u, U_2^u) \doteq (0.53, -0.83)$$

violates the minimum constraint $U_2 \geq 0$ for the unknown U_2, and as the unbounded solution defines the total energy, the unbounded solution U^u lies on the total energy constraint. The bounded solution $U^b \doteq (0.49, 0)$ lies on the boundary $U_2 = 0$ of U_2 lower
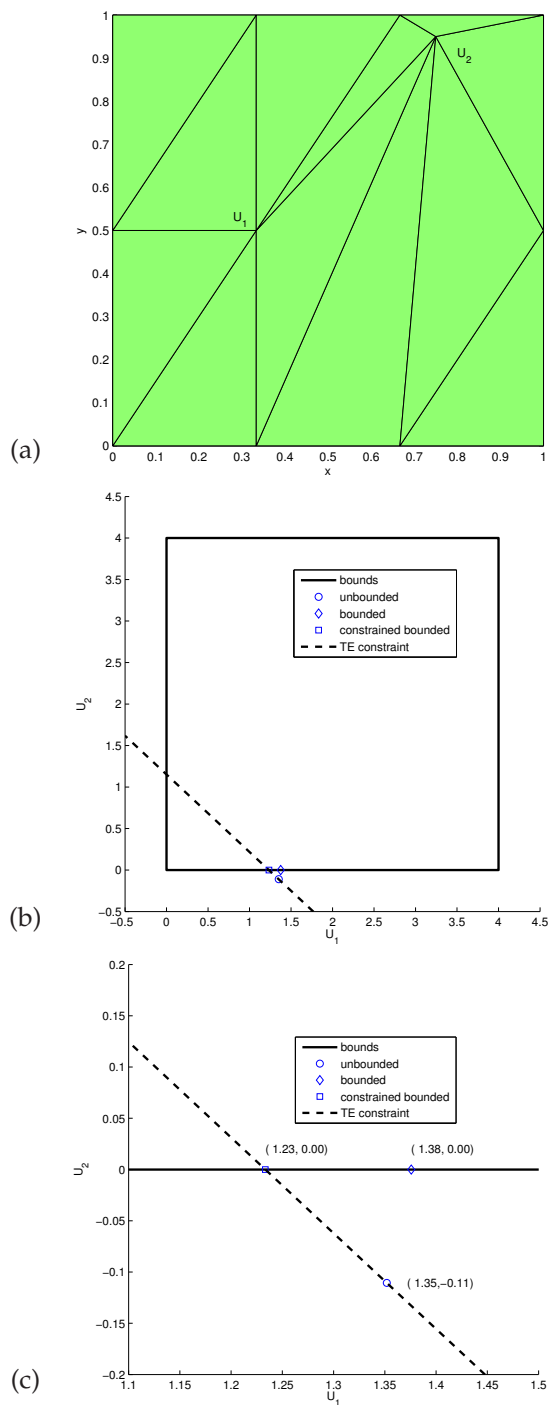
Figure 1: The first simple problem which does have constrained-bounded solution: (a) computational mesh; (b) bounds for two unknowns U_1, U_2, unbounded, bounded, constrained-bounded solutions and total energy constraint in $U_1 \times U_2$ space; (c) zoom of (b) around solutions.
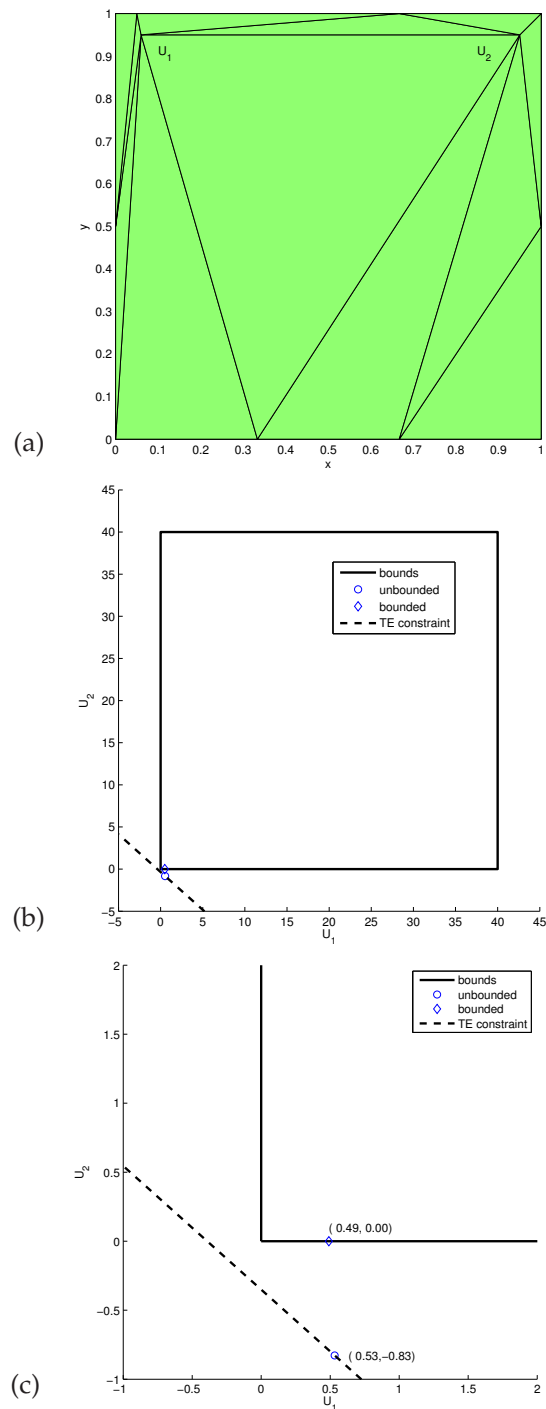
Figure 2: The second simple problem for which repaired and constrained-bounded solution do not exist: (a) computational mesh; (b) bounds for two unknowns U_1, U_2, unbounded, bounded, solutions and total energy constraint in $U_1 \times U_2$ space; (c) zoom of (b) around solutions.

constraint $U_2 \geq 0$. The discrete Dirichlet functional (3.4) values of the unbounded and bounded solutions are

$$\mathcal{F}_h[U^u] \doteq 5439, \quad \mathcal{F}_h[U^b] \doteq 5449.$$

The total energies (3.1) of the unbounded and unbounded solutions are

$$E[U^u] \doteq 14.16, \quad E[U^b] \doteq 14.35.$$

This problem demonstrates that for some very special problems the repaired and constrained-bounded solutions might not exist. However, such problems are really very special and we believe that in real practical simulations repaired and constrained-bounded solutions will always exist.

4.2 Problem with non-smooth anisotropic solution

This problem originates in presentation [26], and its modified version has been used in [6]. The computational region is the unit square with a square hole with size $1/15 \times 1/15$ (the hole is the square $(7/15, 8/15)^2$) in the center shown in Fig. 3(a).

We solve the homogeneous elliptic equation (2.1) with boundary conditions $\psi = 0$ on the outer boundary and $\psi = 2$ on the inner boundary along the hole. The anisotropic conductivity matrix **A** is created by the rotation of the diagonal matrix

$$\mathbf{B} = \begin{pmatrix} 1 & 0 \\ 0 & k \end{pmatrix}, \tag{4.1}$$

where k is a parameter, by the orthogonal matrix **R**

$$\mathbf{R} = \begin{pmatrix} \cos\Theta & -\sin\Theta \\ \sin\Theta & \cos\Theta \end{pmatrix} \tag{4.2}$$

with angle $\Theta = -\pi/3$, so that

$$\mathbf{A} = \mathbf{R} \cdot \mathbf{B} \cdot \mathbf{R}'. \tag{4.3}$$

We use three values of the parameter k, which defines anisotropy ratios $1/k$ of heat conductivity in two orthogonal directions, namely ratios $1/k = 1/25, 1/100$ and $1/1000$.

4.2.1 Uniform meshes

The computational region with the coarsest uniform triangular computational mesh is shown in Fig. 3(b). The triangles are rectangular with the length of their cathetus being equal to $\Delta x = 1/15$. The finer computational meshes are created by uniform refining of the mesh shown in Fig. 3(b) by splitting each triangle into four triangles with vertices at centers of edges of the original triangle. The meshes with the triangles catheti $\Delta x = (1/15, 1/30, 1/60, 1/120, 1/240, 1/480)$ have $(448, 1\,792, 7\,168, 28\,672, 114\,688, 458\,752)$ triangles respectively.
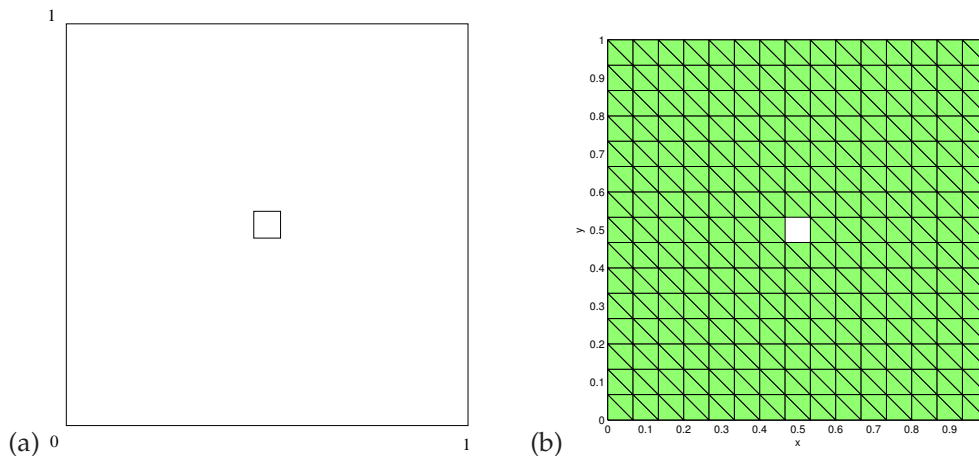
Figure 3: The computational domain (a) and the coarsest uniform computational mesh (b) for problem with non-smooth anisotropic solution.

Table 1: Problem with non-smooth anisotropic solution: minimal values of unbounded numerical solution U^u on the computational domain Ω, L_1 norm of U^u on area $\Omega(U^u < 0)$ where $U^u < 0$ is negative, and the relative size of the area $\Omega(U^u < 0)$ with negative solution in % ; for three anisotropy ratios $1/k = 1/25, 1/100, 1/1000$; and for refining computational mesh. Δx is the length of the cathetus of one triangle.

Δx	ratio $1/k = 1/25$			ratio $1/k = 1/100$			ratio $1/k = 1/1000$		
	$\min_\Omega(U^u)$	$L_{1(U^u)}^{\Omega(U^u<0)}$	$\frac{|\Omega_{(U^u<0)}|}{|\Omega|}$	$\min_\Omega(U^u)$	$L_{1(U^u)}^{\Omega(U^u<0)}$	$\frac{|\Omega_{(U^u<0)}|}{|\Omega|}$	$\min_\Omega(U^u)$	$L_{1(U^u)}^{\Omega(U^u<0)}$	$\frac{|\Omega_{(U^u<0)}|}{|\Omega|}$
1/15	-0.0089	0.00077	13%	-0.029	0.0033	20%	-0.039	0.0047	22%
1/30	-0.0011	0.000069	14%	-0.025	0.0030	28%	-0.048	0.0062	31%
1/60	$-7.0 \cdot 10^{-6}$	$1.3 \cdot 10^{-7}$	4.3%	-0.011	0.0012	33%	-0.053	0.0061	38%
1/120	$-4.5 \cdot 10^{-8}$	$2.1 \cdot 10^{-10}$	3.0%	-0.0004	$2.7 \cdot 10^{-5}$	28%	-0.050	0.0047	41%
1/240	$-3.3 \cdot 10^{-10}$	$3.9 \cdot 10^{-13}$	0.28%	$-1.0 \cdot 10^{-8}$	$2.0 \cdot 10^{-10}$	7.5%	-0.039	0.0028	43%
1/480	$-2.5 \cdot 10^{-12}$	$7.3 \cdot 10^{-16}$	0.07%	$-5.9 \cdot 10^{-13}$	$2.9 \cdot 10^{-15}$	1.9%	-0.020	0.0011	43%

The numerical solutions of these anisotropic problems are shown in Fig. 4 for the anisotropy ratio $1/k = 1/25$, and in Fig. 5 for $1/k = 1/1000$. We present in these figures the unbounded solutions; however, in this style of figures one cannot distinguish different numerical solutions which will be distinguished later. Heat conductivity along the line $y = x/\sqrt{3}$ obtained by rotating y axis by the angle $\Theta = -\pi/3$ is k-times greater than the heat conductivity in the orthogonal direction given by the line $y = -\sqrt{3}x$. This explains the general outlook of the solution decreasing from the boundary value 2 at the hole boundary much faster in direction $y = -\sqrt{3}x$ than in the orthogonal $y = x/\sqrt{3}$ direction. For the ratio $1/k = 1/1000$ the solution along the line $y = -\sqrt{3}x$ is much steeper than that for the ratio $1/k = 1/25$.

The unbounded solutions of this problem for all three anisotropy ratios $1/k = 1/25, 1/100, 1/1000$ have some negative values, thus they are violating the discrete maximum principle (2.8). The minimal negative values of unbounded solutions on refined meshes are presented in Table 1. To quantify how badly the solutions violate the maxi-
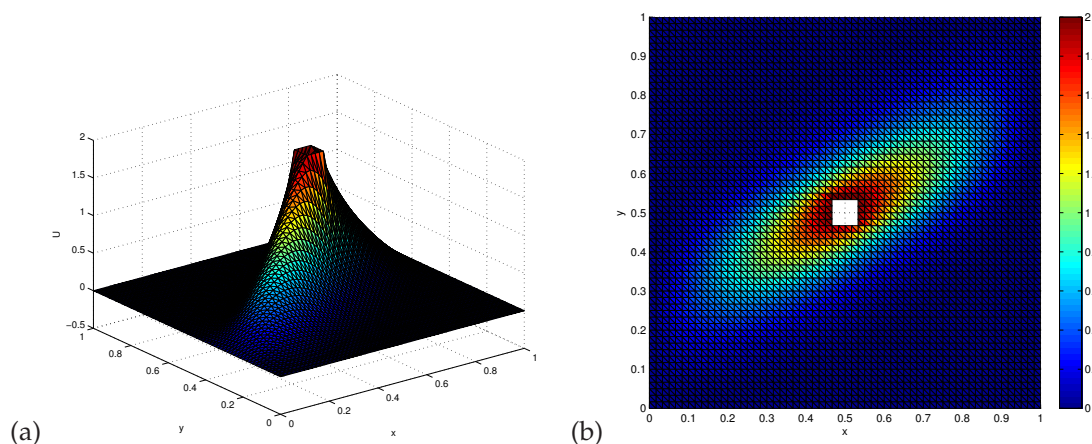
Figure 4: Problem with non-smooth anisotropic solution with anisotropy ratio $1/k=1/25$ ratio on mesh with 60 edges on unit boundary: (a) surface of unbounded solution; (b) colormap of unbounded solution.
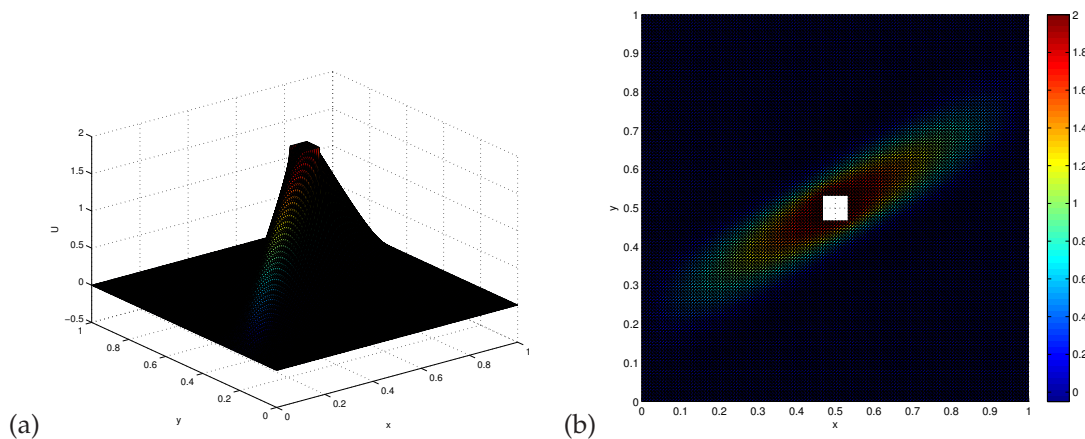

Figure 5: Problem with non-smooth anisotropic solution with anisotropy ratio $1/k=1/1000$ ratio on mesh with 120 edges on unit boundary: (a) surface of unbounded solution; (b) colormap of unbounded solution.

mum principle, we include in Table 1 also L_1 norms of the negative part of solutions, i.e., L_1 norm of the unbounded solutions U^u over the area $\Omega(U^u<0)$ where the unbounded solution $U^u<0$ is negative and relative size in % of this area $\Omega(U^u<0)$. The L_1 norms of the unbounded solutions on the whole domain Ω (to compare with $L_{1(U^u)}^{\Omega(U^u<0)}$ in the table) are $L_1(U^u)=0.220$ for the anisotropy ratio $1/k=1/25$, $L_1(U^u)=0.168$ for $1/k=1/100$ and $L_1(U^u)=0.138$ for $1/k=1/1000$.

Inspecting the table, we notice that for the ratios $1/k=1/25,1/100$ the unbounded solutions seem already to converge to a solution which violates the maximum principle only negligibly. For the ratio $1/k=1/100$, the convergence of the unbounded to a solution violating the maximum principle only negligibly starts later at much finer meshes.

Table 2: Problem with non-smooth anisotropic solution: convergence for the anisotropy ratio $1/k=1/25$: L_1 norm of error (difference from the reference unbounded solution on mesh with $\Delta x=1/480$) and ratios of two successive error norms for the unbounded, bounded, constrained-bounded and repaired solutions.

Δx	unbounded		bounded		constrained-bounded		repaired	
	L_1^{err}	ratio	L_1^{err}	ratio	L_1^{err}	ratio	L_1^{err}	ratio
1/15	0.0925	1.95	0.0921	1.95	0.0909	1.93	0.0914	1.93
1/30	0.0474	2.20	0.0473	2.20	0.0472	2.20	0.0474	2.30
1/60	0.0215	2.40	0.0215	2.40	0.0215	2.40	0.0215	2.40
1/120	0.0090		0.0090		0.0090		0.0090	

Table 3: Problem with non-smooth anisotropic solution: convergence for the anisotropy ratio $1/k=1/100$: L_1 norm of error (difference from the reference unbounded solution on mesh with $\Delta x=1/480$) and ratios of two successive error norms for the unbounded, bounded, constrained-bounded and repaired solutions.

Δx	unbounded		bounded		constrained-bounded		repaired	
	L_1^{err}	ratio	L_1^{err}	ratio	L_1^{err}	ratio	L_1^{err}	ratio
1/15	0.1428	1.66	0.1419	1.68	0.1374	1.71	0.1363	1.70
1/30	0.0858	1.96	0.0844	1.98	0.0804	1.95	0.0804	1.89
1/60	0.0437	2.35	0.0427	2.30	0.0412	2.23	0.0426	2.29
1/120	0.0186		0.0185		0.0185		0.0186	

The exact solution for this problem is not known, so for the convergence study we use the reference unbounded solution computed on the finest mesh with triangles cathetus $\Delta x=1/480$. The convergence for the unbounded, bounded, constrained-bounded, and repaired solutions for meshes with $\Delta x=1/15,1/30,1/60,1/120$ is presented in Table 2 for the anisotropy ratio $1/k=1/25$ and in Table 3 for $1/k=1/100$. The unbounded solutions providing the same results as standard linear FEM is known to converge from theory [19], and the convergence tables also show that the bounded, constrained-bounded and repaired solutions do converge. So the imposed constraints do not destroy the convergence. As the solution is non-smooth, the convergence is only first order. Strictly speaking of course the solution of the elliptic problem is smooth; by non-smooth we mean here that the gradient of the solution in the low conductivity direction changes very fast from very steep to flat. We have not made the convergence study for the anisotropy ratio $1/k=1/1000$, as the unbounded solution on our finest mesh has still rather large error of the order 1% (the relative L_1 norm of negative part of the solution), see Table 1.

To understand the difference in behavior of the solutions for two different ratios $1/k$, we present in Fig. 6 the areas where the unbounded solutions are negative for ratio $1/k=1/25$, and the same in Fig. 7 for ratio $1/k=1/1000$. In both cases for the first four refined meshes with the triangles cathetus $\Delta x=1/15,1/30,1/60,1/120$. The areas with a negative solution are presented by colormaps showing only negative values by different colors
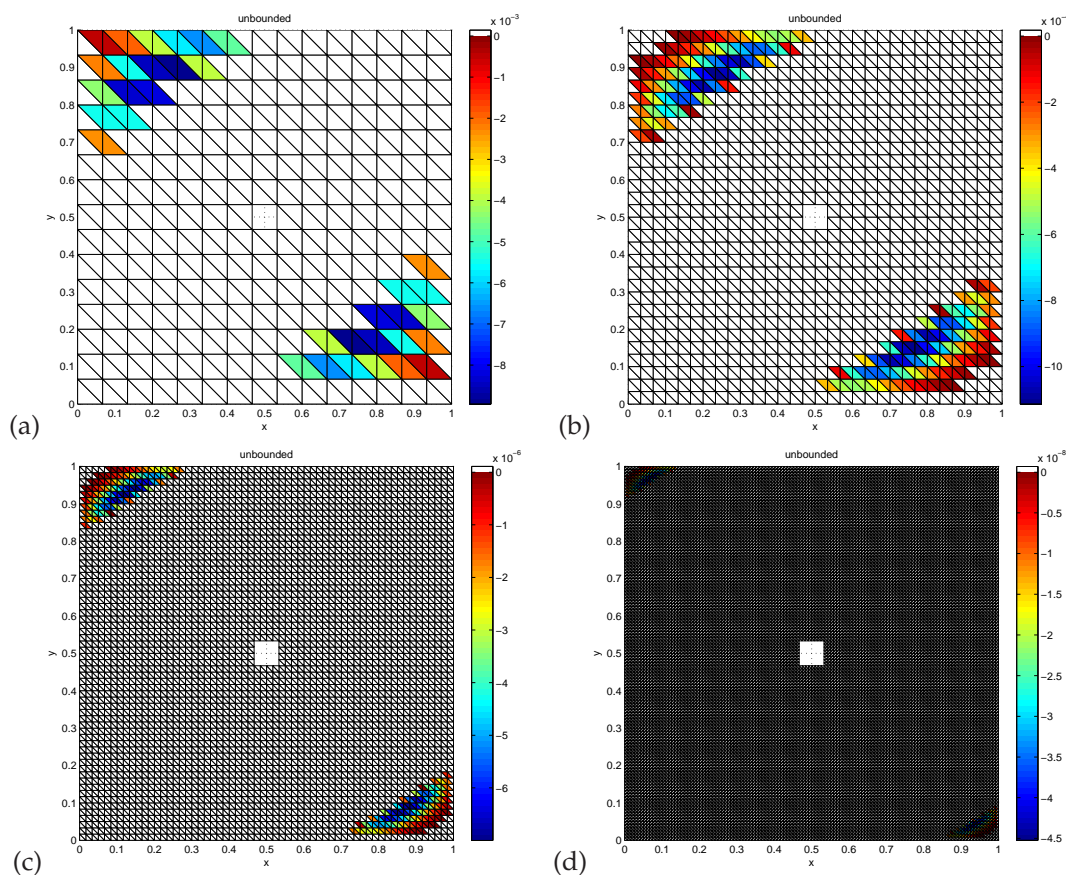
Figure 6: Problem with non-smooth anisotropic solution with anisotropy ratio $1/k = 1/25$, colormaps of unbounded solution showing areas where the solution is negative (areas where the solution is non-negative are white) on: (a) mesh with 15 edges on unit boundary; (b) mesh with 30 edges on unit boundary; (c) mesh with 60 edges on unit boundary; (d) mesh with 120 edges on unit boundary.

and with all positive values presented in white. In Fig. 6 the lower end of the interval for the colormap is given by the minimal negative value presented in Table 1, and the upper end of the interval is zero. The minimal values are increasing towards zero with mesh refinement, and the area where the unbounded solution is negative is getting smaller with refinement. On the other hand, the color map interval for all refinement levels in Fig. 7 for ratio $1/k = 1/1000$ remains (-0.05,0) the regions of negative solutions move towards the solution ridge with refinement creating oscillations. However, the areas of these regions are not getting smaller. It seems that we would need much higher resolution for the unbounded solution to violate less the maximum principle.

To see the differences between different numerical solutions, we have chosen to present 1D cuts of the solutions along the line $y = 7/15$, which is the line defining the lower boundary of the square hole in the solution domain. The 1D cuts are presented for the ratio $1/k = 1/1000$ for which the differences are more visible. Fig. 8 (a),(b) compares
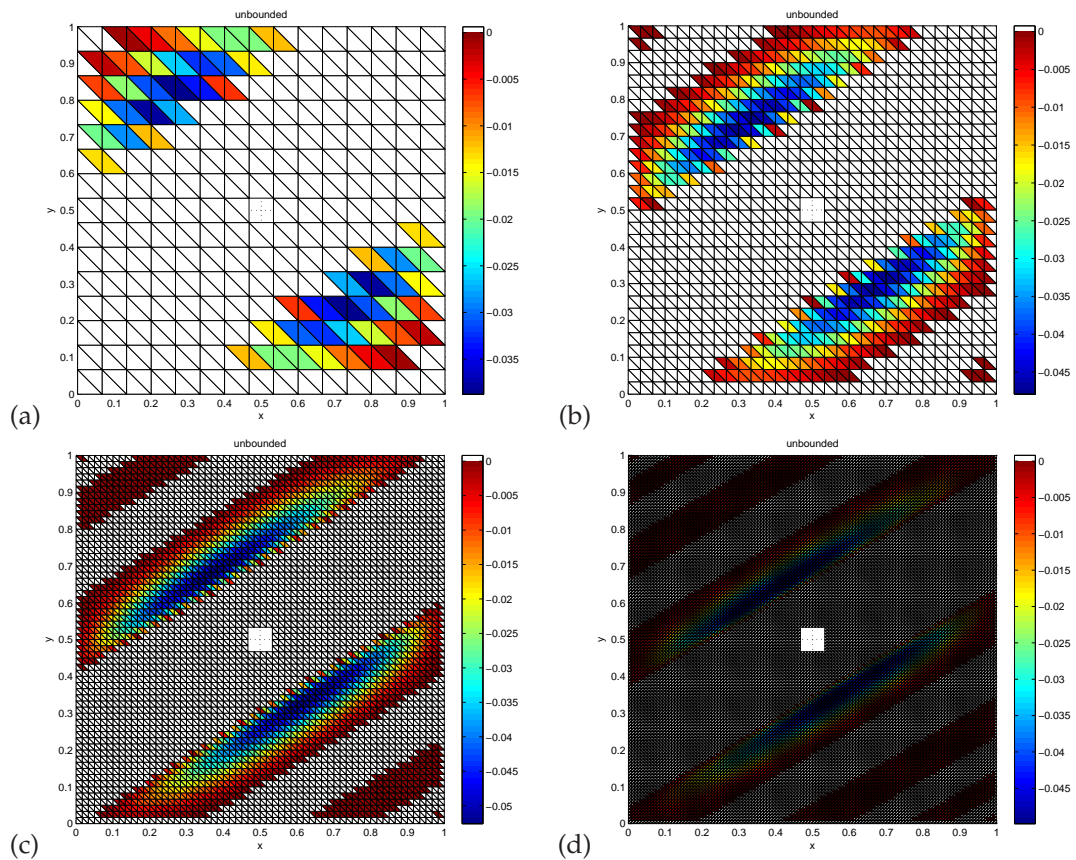
Figure 7: Problem with non-smooth anisotropic solution with anisotropy ratio $1/k = 1/1000$, colormaps of unbounded solution showing areas where the solution is negative (areas where the solution is non-negative are white) on: (a) mesh with 15 edges on unit boundary; (b) mesh with 30 edges on unit boundary; (c) mesh with 60 edges on unit boundary; (d) mesh with 120 edges on unit boundary.

1D cuts of unbounded, bounded, constrained-bounded, and repaired solutions on the finest mesh with 120 cell edges on the outer unit boundary. The unbounded solution is negative in some regions of x. The repaired solution is not smooth with a jump in its gradient which is clearly bad as the solution of the Laplace equation should have a smooth gradient. The best seem to be the bounded and constrained-bounded solutions which are quite close to each other. They are smooth and positive, i.e., satisfy the maximum principle. To show the oscillations (from the positive to negative values) of the solution along the diagonal $y = 1-x$ visible in the solution on the finest mesh in Fig. 7(d), in Fig. 8(c) we present the 1D cut of this solution on the finest mesh with 120 edges on unit boundary. In Fig. 8(c) the solid line presents the unbounded solution U^u plotted in the standard linear scale and the dashed line presents absolute value $|U^u|$ of the unbounded solution in the logarithmic scale. Each sharp local minimum on this logarithmic plot corresponds to one change of the sign of U^u where its value passes through zero and the absolute value
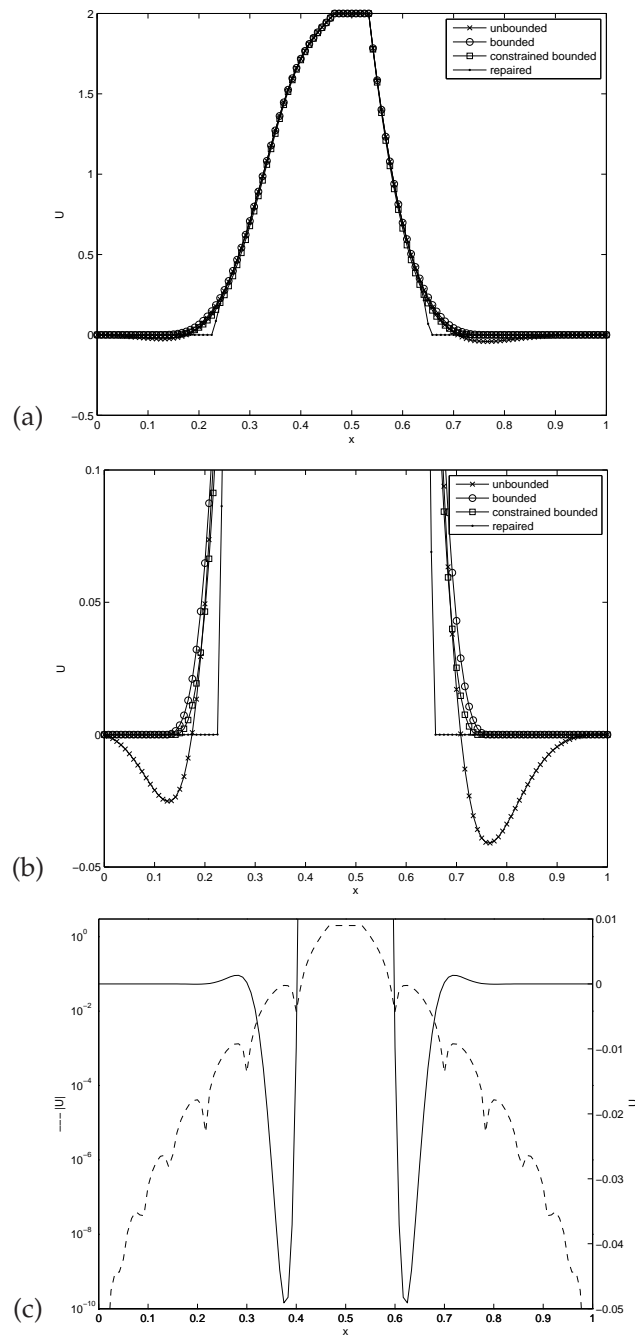
Figure 8: Problem with non-smooth anisotropic solution with the anisotropy ratio $1/k = 1/1000$ on the mesh with 120 edges on unit boundary: (a) full view and (b) view zoomed, scaled in y direction of 1D cuts along the line $y = 7/15$, comparison of unbounded, bounded, constrained-bounded and repaired solution; (c) 1D cut of unbounded solution U^u along the diagonal $y = 1 - x$, the solid line is U^u with the right linear axis and the dashed line is $|U^u|$ with the left logarithmic axis.
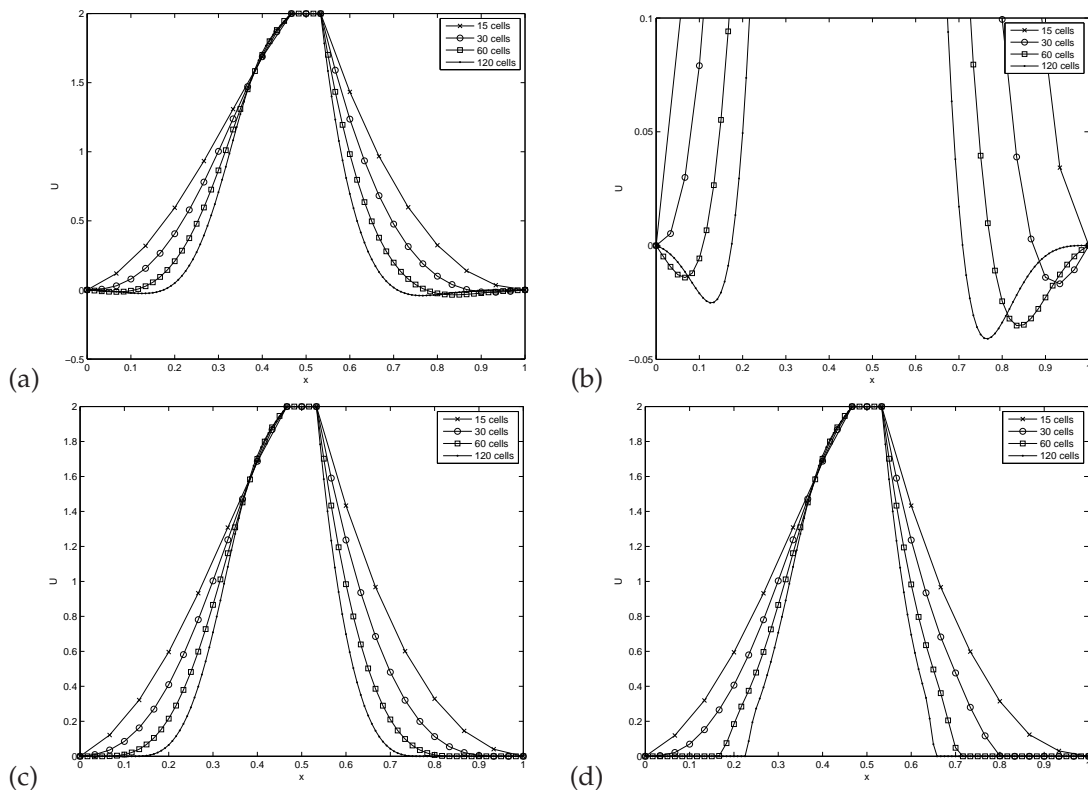
Figure 9: Problem with non-smooth anisotropic solution with anisotropy ratio $1/k=1/1000$, 1D cuts along the line $y=7/15$, convergence with 15, 30, 60 and 120 edges on unit boundary of: (a) unbounded; (b) zoomed view of unbounded, scaled in y direction; (c) bounded; (d) repaired solutions.

(necessary for logarithmic scale) introduces discontinuity in the first derivative. Fig. 9 presents convergence of 1D cuts for unbounded, zoomed unbounded, bounded, and repaired solutions with mesh refined from 15 to 120 cell edges on the outer unit boundary. The constrained-bounded solutions are very close to the bounded solutions, so that one is unable to distinguish them on such 1D cuts plots. The solutions are not converged yet; for converged solution we would need higher resolution. We might notice an incorrect inflection point in the finest resolution (120 cells in red) of repaired solution in Fig. 9(d).

4.2.2 Non-uniform meshes

To show that our approach works also on non-uniform meshes, we have chosen two non-uniform triangulations of the computational domain shown in Fig. 3(a). The first mesh is created by random movements of the nodes (by $r\Delta x/2$ where Δx is the length of cathetus of uniform triangles and $r \in (0,1)$ is a random number) of the uniform mesh (and its uniform refinements) shown in Fig. 3(b). The second non-uniform mesh is the unstructured mesh generated by PLTMG [27] package for the computational domain shown in Fig. 3(a).
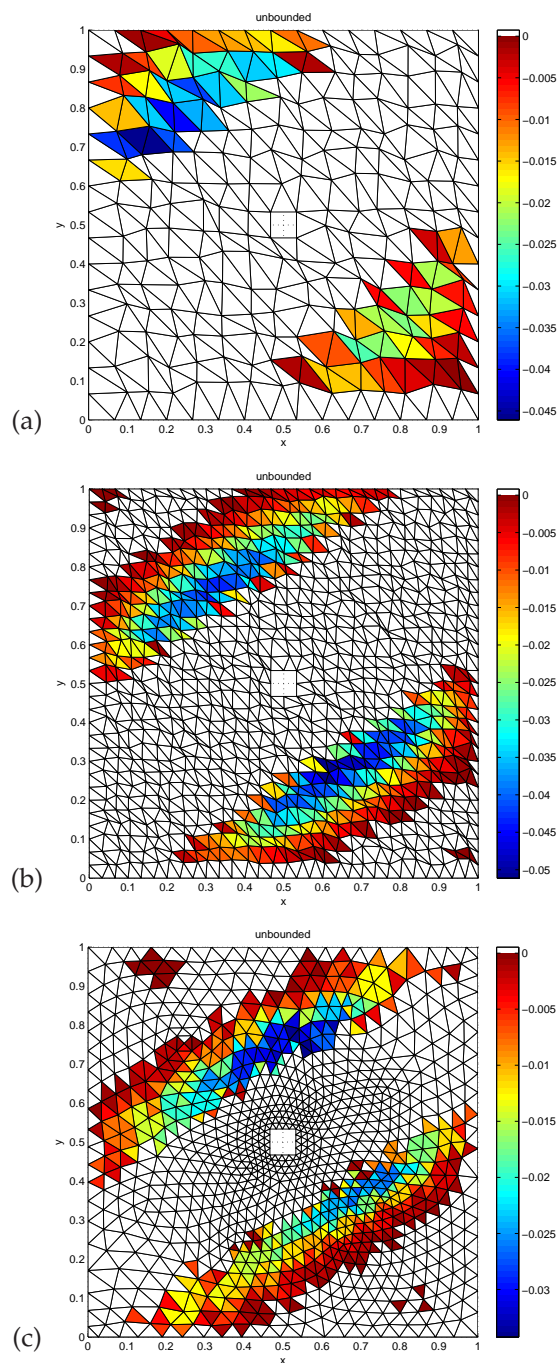
Figure 10: Problem with non-smooth anisotropic solution with anisotropy ratio $1/k = 1/1000$, colormaps of unbounded solution showing areas where the solution is negative (areas where the solution is non-negative are white) on: (a) randomly perturbed uniform mesh with 15 edges on unit boundary; (b) randomly perturbed uniform mesh with 30 edges on unit boundary; (c) PLTMG generated mesh.

Table 4: Problem with non-smooth anisotropic solution with anisotropy ratio $1/k = 1/100$ on unstructured meshes: minimal values of unbounded numerical solution U^u on the computational domain Ω, L_1 norm of U^u on area $\Omega(U^u < 0)$ where $U^u < 0$ is negative, and the relative size of the area $\Omega(U^u < 0)$ with negative solution in % ; for refining computational meshes. The L_1 norm of the unbounded reference solution (with $\Delta x = 1/480$) on the whole domain Ω on the uniform mesh (to compare with $L_{1(U^u)}^{\Omega(U^u<0)}$ in the table) is $L_1(U^u) = 0.168$.

Nr. of triangles	$\min_\Omega(U^u)$	$L_{1(U^u)}^{\Omega(U^u<0)}$	$\frac{|\Omega_{(U^u<0)}|}{|\Omega|}$
112	-0.001	$2.1 \cdot 10^{-5}$	5.9 %
448	-0.011	$3.8 \cdot 10^{-4}$	27 %
1792	-0.0033	$2.3 \cdot 10^{-4}$	31 %
7168	-0.0003	$1.1 \cdot 10^{-5}$	25 %
28672	$-1.8 \cdot 10^{-6}$	$2.1 \cdot 10^{-8}$	7.1 %

Again, the unbounded solutions on such meshes violate the maximum principle while the bounded, constrained-bounded, and repaired do not violate the maximum principle. The general shape of solution remains the same and corresponds approximately (depending on mesh resolution) to that for the uniform mesh presented in Figs. 4 and 5. We present here only the colormaps of areas with negative solution (violating the maximum principle) for two randomly perturbed uniform meshes and for one unstructured PLTMG mesh in Fig. 10 for the anisotropy ratio $k = 1/1000$.

The minimal negative values of unbounded solutions on refined unstructured meshes for the anisotropy ratio $1/k = 1/100$ are presented in Table 4. To quantify how badly the solutions violate the maximum principle, we included in Table 4 also L_1 norms of negative part of solutions, i.e., L_1 norm of unbounded solutions U^u over area $\Omega(U^u < 0)$ where $U^u < 0$ is negative and relative size in % of the area $\Omega(U^u < 0)$ where the solution is negative. As the unstructured meshes have more smaller triangles around the central hole, the unbounded solutions on these meshes violate the maximum principle less than that on uniform meshes with the same number of triangles, compare with Table 1 for uniform triangulations, where the meshes with uniform triangle catheti $\Delta x = (1/15, 1/30, 1/60, 1/120)$ have (448, 1 792, 7 168, 28 672) triangles, respectively.

5   Numerical experiments for non-homogeneous equation

In this section we will present several numerical tests solving the Poisson equation (2.1) with non-negative sources $f \geq 0$ and zero Dirichlet boundary conditions $\psi = 0$. The maximum principle for $f \geq 0$ (2.5) and $\psi = 0$ implies that the solution has to be non-negative $u \geq 0$ everywhere. The presented tests violate this maximum principle for the unbounded solution which is exactly the same as the standard linear finite element solution. Below, we present only numerical results of the unbounded solutions. The bounded, constrained-bounded, and repaired solutions for all the presented problems satisfy the discrete maximum principle (2.8), i.e., are non-negative everywhere.

5.1   Simple isotropic problem

This is simple isotropic problem taken from [13]. Matrix $\mathbf{A}$ is identity $\mathbf{A} = \mathbf{I}$. Computational domain is $\Omega = [0,1] \times [0,0.3]$. The source is defined as follows $f(x,y) = 1$ for $(x,y) \in [0,0.5] \times [0,0.075]$ and $f(x,y) = 0$ elsewhere. The zero Dirichlet boundary conditions are specified on the boundary. The mesh is created by putting a uniform 4×4 rectangular mesh on the domain Ω and splitting each rectangle into four triangles along its two diagonals, see Fig. 11(b). The triangulation is not acute. The solution of this problem is not known, but as $-\operatorname{div}\mathbf{grad}u = f \geq 0$ everywhere, then the maximum principle (2.5) implies that the minimum of the solution is on the boundary; so due to zero Dirichlet boundary conditions the solution has to be non-negative everywhere. The unbounded solution of this problem has values in the interval $(-4.21 \cdot 10^{-5}, 2.24 \cdot 10^{-3})$ violating the maximum principle in 3 nodes (12 % of the domain), with L_1 norm of the negative part of the solution being $6.04 \cdot 10^{-7}$ (L_1 norm of the unbounded solution is $1.30 \cdot 10^{-4}$).

5.2   Strong uniform anisotropy with central source

In this problem computational domain is unit square $\Omega = [0,1]^2$. The anisotropic diffusion matrix $\mathbf{A}$ is the same as in the problem with non-smooth anisotropic solution (4.3) with $\Theta = -\pi/3$ and the anisotropic ratio $1/k = 1/100$. The source $f(x,y)$ is $f(x,y) = 10^5$ inside the central region $(x,y) \in [0.45, 0.55]^2$ and zero outside the central region. The zero Dirichlet boundary conditions are applied on the boundary.

We use the mesh with the same structure as the mesh for the problem with non-smooth anisotropic solution (presented in Section 4.2) shown in Fig. 3(b), but just without the hole, with 60 triangle catheti on one $[0,1]$ side, see Fig. 12(b). The shape of the solution of this problem presented in Fig. 12(a) is close to the shape of the solution of the problem with non-smooth anisotropic solution shown in Fig. 5. The maximum principle implies that the solution has to be non-negative, however, the unbounded solution U^u produces a negative solution in quite a large area, as shown in Fig. 12(b). The values of unbounded solution are from interval $U^u \in (-0.097, 18)$, the unbounded solution is negative in 1262 nodes (36 %) out of the total 3481 internal nodes, and the L_1 norm of the negative part of the unbounded solution $L_1(U^u)_{\Omega(U^u < 0)}$ is 0.01 (L_1 norm of the unbounded solution is 1.7). These data, which characterize how much the DMP has been violated, for this problem solved on both coarser and finer meshes are presented in Table 5.

5.3   Non uniform anisotropy

This problem is taken from [3]. Computational domain is the square $\Omega = [0,0.5]^2$. The anisotropic diffusion matrix $\mathbf{A}(x,y)$ depends here on the position (x,y) and is given by

$$\mathbf{A}(x,y) = \begin{pmatrix} y^2 + \epsilon x^2 & -(1-\epsilon)xy \\ -(1-\epsilon)xy & x^2 + \epsilon y^2 \end{pmatrix} \tag{5.1}$$
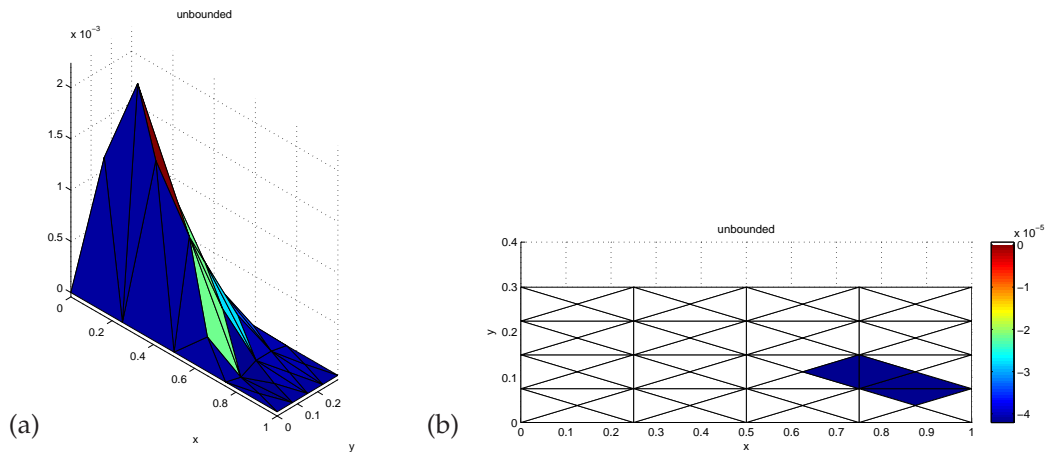
Figure 11: Simple isotropic Poisson equation problem: (a) surface of unbounded solution; (b) colormap of unbounded solution showing areas of negative solution.
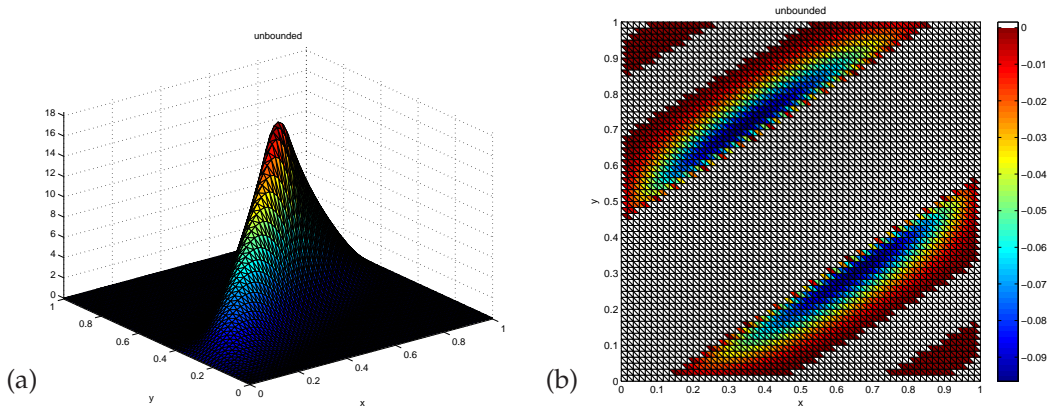

Figure 12: Strong uniform anisotropy $1/k = 1/100$ ratio, central source Poisson equation problem on uniform mesh with 60 edges on unit boundary: (a) surface of unbounded solution; (b) colormap of unbounded solution showing areas of negative solution.

Table 5: Strong uniform anisotropy $1/k = 1/100$ ratio, central source Poisson equation problem on refined uniform meshes: minimal values of unbounded numerical solution U^u on the computational domain Ω, L_1 norm of U^u on area $\Omega(U^u < 0)$ where $U^u < 0$ is negative, and the relative size of the area $\Omega(U^u < 0)$ with negative solution in % ; for refining computational meshes. The L_1 norm of the unbounded reference solution (with $\Delta x = 1/240$) on the whole domain Ω (to compare with $L_{1(U^u)}^{\Omega(U^u<0)}$ in the table) is $L_1(U^u) = 1.65$.

Δx	$\min_\Omega(U^u)$	$\max_\Omega(U^u)$	$L_{1(U^u)}^{\Omega(U^u<0)}$	$\frac{|\Omega_{(U^u<0)}|}{|\Omega|}$
1/15	-0.070	4.8	-0.0079	23%
1/30	-0.17	15	-0.0214	31%
1/60	-0.097	18	-0.0106	35%
1/120	-0.0031	21	$-2.4\cdot10^{-4}$	29%
1/240	$-8.4\cdot10^{-8}$	22	-1.610^{-9}	7.9%

with $\epsilon = 10^{-3}$ which gives the anisotropy ratio. The source $f(x,y)$ is $f(x,y)=1$ for $(x,y) \in [0.125,0.375]^2$ and zero otherwise. The zero Dirichlet boundary conditions are applied on the boundary.

For this problem we use the triangular mesh obtained from the uniform orthogonal mesh of 30×30 squares by splitting each square cell into four triangles by two diagonals of the square, see Fig. 13(b). The surface plot of the unbound solution to this problem is shown in Fig. 13(a). The maximum principle (2.5) implies that the solution has to be non-negative, however the unbounded solution U^u produces a negative solution in quite a large area, as shown in Fig. 13(b). The values of unbounded solution are from interval $U^u \in (-2.010^{-3}, 0.26)$, the unbounded solution is negative in 209 nodes (12 %) out of the total 1741 internal nodes, and the L_1 norm of the negative part of the unbounded solution $L_1(U^u)_{\Omega(U^u<0)}$ is $8.1 \cdot 10^{-6}$ (L_1 norm of the unbounded solution is 0.019).

5.4 Non uniform rotating anisotropy

For this problem computational domain is unit square $\Omega = [0,1]^2$. The anisotropic diffusion matrix $\mathbf{A}(x,y)$ depends on the position (x,y) and is given by the rotation of the diagonal matrix (4.1) around the origin by the angle φ which is the angular polar coordinate of the point (x,y):

$$\mathbf{A}(x,y) = \begin{pmatrix} \cos\varphi & -\sin\varphi \\ \sin\varphi & \cos\varphi \end{pmatrix} \cdot \begin{pmatrix} 1 & 0 \\ 0 & k \end{pmatrix} \cdot \begin{pmatrix} \cos\varphi & \sin\varphi \\ -\sin\varphi & \cos\varphi \end{pmatrix} \tag{5.2}$$

with $k = 1000$ which gives the anisotropy ratio and

$$\cos\varphi = x/r, \quad \sin\varphi = y/r, \quad r = \sqrt{x^2 + y^2}.$$

The source $f(x,y)$ is $f(x,y) = 10^5$ for $(x,y) \in (0.7,0.8) \times (0,0.1)$ and zero elsewhere. The zero Dirichlet boundary conditions are applied on the boundary.

For this problem we use the triangular mesh obtained from the uniform orthogonal mesh of 20×20 squares by splitting each square cell into four triangles by two diagonals of the square, see Fig. 14(b). The surface plot of the unbounded solution to this problem is shown in Fig. 14(a). The maximum principle implies that the solution has to be non-negative, however, the unbounded solution U^u produces a negative solution in quite a large area, as shown in Fig. 14(b). The values of unbounded solution are from interval $U^u \in (-0.015, 0.47)$, the unbounded solution is negative in 354 nodes (46 %) out of the total 761 internal nodes, and the L_1 norm of the negative part of the unbounded solution $L_1(U^u)_{\Omega(U^u<0)}$ is 1.310^{-3} (L_1 norm of the unbounded solution is 0.031).

6 Conclusion

We have proposed two new methods for enforcing discrete maximum principle for linear finite element solutions on 2D triangular mesh of the linear second-order self-adjoint
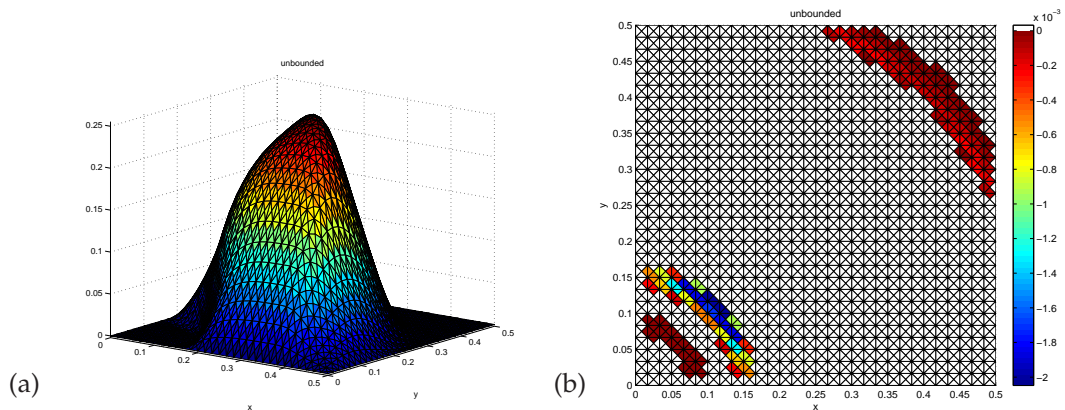
Figure 13: Non uniform anisotropy Poisson equation problem: (a) surface of unbounded solution; (b) colormap of unbounded solution showing areas of negative solution.
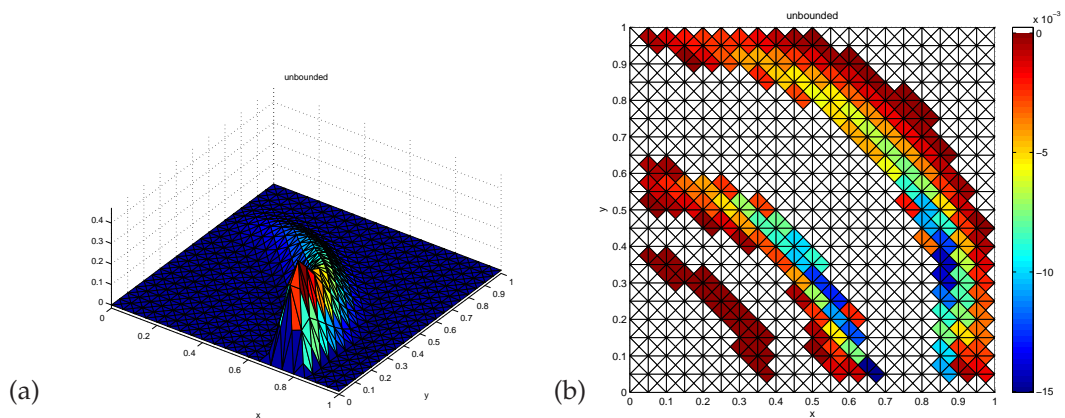

Figure 14: Non uniform rotating anisotropy Poisson equation problem on uniform mesh: (a) surface of unbounded solution; (b) colormap of unbounded solution showing areas of negative solution.

elliptic equation without lower-order terms.

First approach is based on repair technique, which is a posteriori correction of the discrete solution. Second method is based on constrained optimization.

Numerical experiments demonstrate the ability of the new methods to produce numerical solutions satisfying the discrete maximum principle, contrary to the standard linear finite element method.

Numerical experiments also show that convergence rate of new methods is about the same as for original linear finite element method.

In the future we plan to analyze method using constrained optimization with respect to its performance. We hope that we will be able to develop more practical method taking into account that we are solving very special quadratic optimization problem with very simple constraints. We also planning to extend optimization method to the case of mixed finite element [29] and mimetic discretizations [28].

Acknowledgments

References

[1] A. Draganescu, T. F. Dupont and L. R. Scott, Failure of the discrete maximum principle for an elliptic finite element problem, Math. Comput., 74(249) (2005), 1-23.
[2] C. Le Potier, Finite volume scheme for highly anisotropic diffusion operators on unstructured meshes, CR Acad. Sci. I–Math., 340(12) (2005), 921-926.
[3] C. Le Potier, Finite volume monotone scheme for highly anisotropic diffusion operators on unstructured triangular meshes, CR Acad. Sci. I–Math., 341(12) (2005), 787-792, 2005.
[4] J. Droniou and R. Eymard, A mixed finite volume scheme for anisotropic diffusion problems on any grid, Numer. Math., 105(1) (2006), 35-71.
[5] M. J. Mlacnik and L. J. Durlofsky, Unstructured grid optimization for improved monotonicity of discrete solutions of elliptic equations with highly anisotropic coefficients, J. Comput. Phys., 216(1) (2006), 337-361.
[6] K. Lipnikov, M. Shashkov, D. Svyatskiy and Y. Vassilevski, Monotone finite volume schemes for diffusion equations on unstructured triangular and shape-regular polygonal meshes, J. Comput. Phys., 227(1) (2007), 492-512.
[7] J. M. Nordbotten, I. Aavatsmark and G. T. Eigestad, Monotonicity of control volume methods, Numer. Math., 106(2) (2007), 255-288.
[8] P. G. Ciarlet and P. A. Raviart, Maximum principle and uniform convergence for the finite element method, Comput. Method. Appl. Mech. Engrg., 2(1) (1973), 17-31.
[9] M. Krizek and L. Liu, Finite element approximation of a nonlinear heat conduction problem in anisotropic media, Comput. Method. Appl. Mech. Engrg., 157(3-4) (1998), 387-397.
[10] M. Krizek and L. P. Liu, On the maximum and comparison principles for a steady-state nonlinear heat conduction problem, Z. Angew. Math. Mech., 83(8) (2003), 559-563.
[11] J. Karatson and S. Korotov, Discrete maximum principles for finite element solutions of nonlinear elliptic problems with mixed boundary conditions, Numer. Math., 99(4) (2005), 669-698.
[12] J. Karatson and S. Korotov, Discrete maximum principles for finite element solutions of some mixed nonlinear elliptic problems using quadratures, J. Comput. Appl. Math., 192(1) (2006), 75-88.
[13] E. Burman and A. Ern, Discrete maximum principle for galerkin approximations of the laplace operator on arbitrary meshes, CR Acad. Sci. I–Math., 338(8) (2004), 641-646.
[14] T. Vejchodsky and P. Solin, Discrete maximum principle for a problem with piecewise-constant coefficients solved by hp-fem, Technical Report 2006-10, University of Texas at El Paso, Dept. of Mathematical Sciences, 2006.

[15] S. Deng, K. Ito and Z. Li, Three-dimensional elliptic solvers for interface problems and applications, J. Comput. Phys., 184(1) (2003), 215-243.

[16] H. Hoteit, R. Mose, B. Philippe, P. Ackerer and J. Erhel, The maximum principle violations of the mixed-hybrid finite-element method applied to diffusion equations, Int. J. Numer. Meth. Eng., 55(12) (2002), 1373-1390.

[17] J. C. Strikwerda, Finite Difference Schemes and Partial Differential Equations, Wadsworth, Inc., Belmont, 1989.

[18] M. Shashkov, Conservative Finite-Difference Methods on General Grids, CRC Press, Boca Raton, Florida, 1996.

[19] P. G. Ciarlet, Basic error estimates for elliptic problems, in: P. G. Ciarlet and J. L. Lions (Eds.), Handbook of Numerical Analysis, Volume II: Finite Element Methods (Part 1), Elsevier, 1990.

[20] M. Kuchařík, M. Shashkov and B. Wendroff, An efficient linearity-and-bound-preserving remapping method, J. Comput. Phys., 188(2) (2003), 462-471.

[21] M. Shashkov and B. Wendroff, The repair paradigm and application to conservation laws, J. Comput. Phys., 198(1) (2004), 265-277.

[22] R. L. Loubere, M. Staley and B. Wendroff, The repair paradigm: New algorithms and applications to compressible flow, J. Comput. Phys., 211(2) (2006), 385-404.

[23] K. Schittkowski, QL: A Fortran code for convex quadratic programming – user's guide, Technical Report, University of Bayreuth, 2003.

[24] M. J. D. Powell, On the quadratic programming algorithm of Goldfarb and Idnani, Technical Report DAMTP 1983/Na 19, University of Cambridge, Cambridge, 1983.

[25] D. Goldfarb and A. Idnani, A numerically stable method for solving strictly convex quadratic programs, Math. Program., 27 (1983), 1-33.

[26] M. Mlacnik, L. Durlofsky, R. Juanes and H. Tchelepi, Multipoint flux approximations for reservoir simulation, 12th Annual SUPRI-HW Meeting, November 18-19, Stanford University, 2004.

[27] R. E. Bank, PLTMG: A Software Package for Solving Elliptic Partial Differential Equations. Users' Guide 8.0, SIAM Publisher, Philadelphia, 1998.

[28] J. Hyman, M. Shashkov and S. Steinberg, The numerical solution of diffusion problems in strongly heterogeneous non-isotropic materials, J. Comput. Phys., 132 (1997), 130-148.

[29] F. Brezzi and M. Fortin, Mixed and Hybrid Finite Element Methods, Springer-Verlag, New York, 1991.